Solution Structure of a Natural CPPC Active Site Variant, the Reduced Form of Thioredoxin *h*1 from Poplar[†,‡]

Nicolas Coudevylle,[§] Aurélien Thureau,[§] Christine Hemmerlin,[§] Eric Gelhaye,[||] Jean-Pierre Jacquot,[||] and Manh-Thong Cung*[,§]

Laboratoire de Chimie-Physique Macromoléculaire, UMR 7568 CNRS-INPL, Groupe ENSIC, 1 rue Grandville, B.P. 451, 54001 Nancy Cedex, France, and Laboratoire Interaction Arbres Microorganismes, UMR 1136 INRA-UHP, IFR 110 Génomique, Ecophysiologie et Ecologie Fonctionnelles, Université Henri Poincaré Nancy-1, B.P. 239, 54506 Vandoeuvre Cedex, France

Received October 12, 2004; Revised Manuscript Received December 2, 2004

ABSTRACT: Assignment of heteronuclear and homonuclear multidimensional NMR spectra permits determination of the first three-dimensional solution structure of a higher-plant thioredoxin *h*. The collection of 1906 distance restraints, 137 TALOS-derived dihedral restraints, and 66 hydrogen bonds was used in the restrained molecular dynamics protocol to calculate the structure of the reduced form of thioredoxin *h*1 from poplar with an atomic rmsd of 0.60 ± 0.12 Å. This enzyme exhibits an unusual active site with the sequence WCPPC and original properties in terms of stability and specificity. Compared to other known thioredoxin structures, thioredoxin *h*1 from poplar adopts the classical "Trx fold". Its atypical active site possesses a conformation similar to that of other common thioredoxins but appears to be more rigid. Moreover, the hydrogen bond network, stabilizing the in-core β-sheet, is tighter than in *Chlamydomonas reinhardtii*, explaining the difference in thermostability.

Thioredoxins (Trxs)[1] belong to a superfamily of oxidoreductases, the function of which is either to create disulfide bonds (protein disulfide isomerases) or to reduce disulfide bonds (glutaredoxins and thioredoxins) (*1*). Thioredoxins are ubiquitous small proteins (ca. 120 amino acids in the mature form), generally very stable, and excellent catalysts for disulfide reduction. Although thioredoxins can be quite divergent in their primary structure, they seem to be related, at the three-dimensional level, to all proteins characterized so far possessing a similar architecture, named the thioredoxin fold (*2*). Genome sequencing has revealed that there are numerous thioredoxin genes in plants (at least 20 in *Arabidopsis thaliana*) (*3*).

The *h* class of thioredoxins is specific to plant organisms. It represents a large multigenic family involved in various processes as protection against oxidative stress and carbon and nitrogen metabolism regulation, but their exact role and cellular distribution remain unclear at least for some isoforms. In higher plants, several members of a subgroup of thioredoxin *h*, called subgroup I (*4*), present unique functional and structural features as a variant active site with two Cys residues and the sequence WCPPC. These "CPPC enzymes" have been studied biochemically in vitro with the poplar and *Arabidopsis* proteins, and found to possess catalytic properties similar to those of the CGPC enzymes (*5*, *6*). The use of yeast mutants suggests, however, that the CPPC enzymes may act specifically in some oxidoreduction reactions, including sulfate assimilation, where they cannot be replaced with the CGPC isoforms (*7*). No structural study has been reported about thioredoxin *h* from higher plants, but the closest structure known is that of *Chlamydomonas reinhardtii* (*8*), the sequence of which is only 53% identical with that of poplar thioredoxin *h*1. Thus, to understand the consequence of the G to P mutation for the structure, properties, and specificity of thioredoxin, we have overexpressed poplar thioredoxin *h*1 (PtTrx*h*1) and purified isotopically labeled samples. We report here the first structure of a higher-plant thioredoxin *h*, determined by NMR spectroscopy, and the structural comparison with other thioredoxins possessing the more classical CGPC active site.

As a first step in this study, we recently reported the near-complete (97%) ^{1}H, ^{13}C, and ^{15}N chemical shift assignment of reduced thioredoxin *h*1 from poplar (*9*). These chemical shifts were deposited in the BioMagResBank as entry BMRB-6079.

MATERIALS AND METHODS

Sample Preparation. The coding sequence of thioredoxin *h*1 from *Populus tremula* was cloned into the pET-Trxh1 expression vector and used to modify the expression of *Escherichia coli* strain BL21. The ^{15}N- and ^{13}C-labeled

[†] This research was supported by the CNRS, the Universities of Nancy I, and INPL.

[‡] Atomic coordinates and NMR-derived restraints have been deposited in the Protein Data Bank (entry 1TI3).

* To whom correspondence should be addressed. Phone: 33 (0)3 83 17 51 07. Fax: 33 (0)3 83 37 99 77. E-mail: Manh-Thong.Cung@ensic.inpl-nancy.fr.

[§] UMR 7568 CNRS-INPL.

[||] Université Henri Poincaré Nancy-1.

[1] Abbreviations: CrTrx*h*1, *C. reinhardtii* thioredoxin *h*; HSQC, heteronuclear single-quantum coherence; NMR, nuclear magnetic resonance; NOE, nuclear Overhauser effect; NOESY, NOE spectroscopy; rmsd, root-mean-square deviation; PtTrx*h*1, poplar thioredoxin *h*1; Trx, thioredoxin; TSP-d_4, trimethylsilyl-3-propionic acid-2,2,3,3-d_4, sodium salt.

10.1021/bi047816n CCC: $30.25
Published on Web 01/21/2005

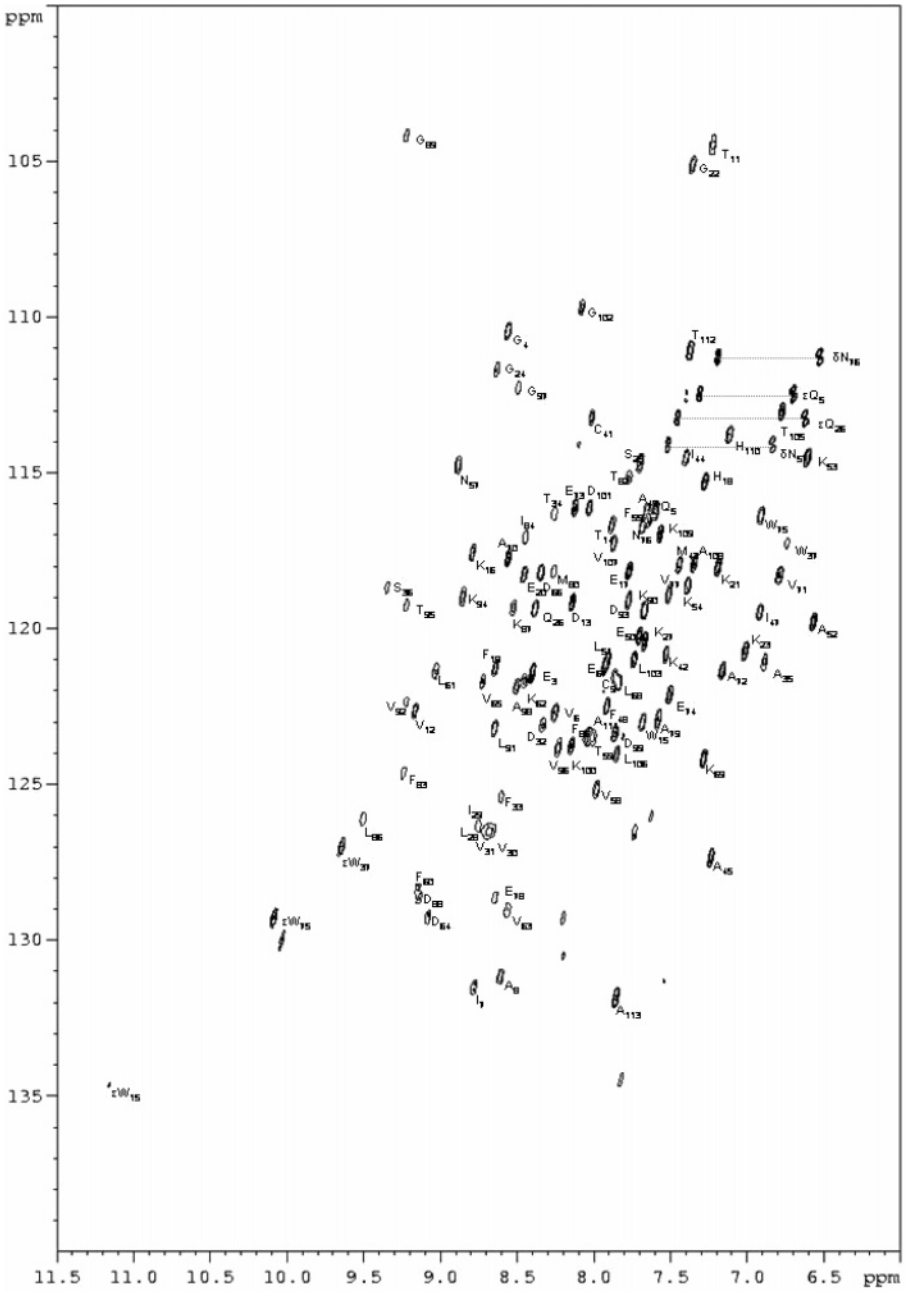

FIGURE 1: $^{1}H-^{15}N$ HSQC spectrum of the reduced form of thioredoxin *h*1 from poplar uniformly labeled with ^{15}N and ^{13}C, recorded at a ^{1}H frequency of 600 MHz, 1.85 mM, in a 95% H_2O/5% D_2O mixture, with 50 mM phosphate buffer (pH 5.9) at 298 K.

sample was prepared by growing cells at 37 °C in minimal medium M9, supplemented with $^{15}NH_4Cl$ (Cambridge Isotope Laboratories) as the sole nitrogen source and with ^{13}C-labeled glucose (Cambridge Isotope Laboratories) as the only carbon source. Purification and concentration were carried out as described by Behm and Jacquot (*5*). The sample purity and molecular mass (12 444 Da for 113 residues) were checked by SDS−PAGE and electrospray mass spectrometry, respectively.

The uniformly ^{15}N- and ^{13}C-labeled NMR sample had a protein concentration of 1.85 mM (95% H_2O and 5% D_2O) in 50 mM phosphate buffer and 10 mM 1,5-dithiothreitol-d_{10} (Cambridge Isotope Laboratories) (pH 5.9) and sealed under argon.

NMR Spectroscopy and Experimental Restraints. All spectra were acquired at 298 K on a Bruker DRX 600 MHz spectrometer equipped with a gradient three-axis TXI probe. Spectra were processed using XWINNMR (Bruker) and analyzed with XEASY (*10*). TSP-d_4 (Euriso-top) was used as an internal reference for ^{1}H chemical shifts and as external reference for calibration of ^{13}C chemical shifts. Indirect referencing was used for the ^{15}N chemical shift (*11*). Backbone amide $^{1}H^{N}$, $^{1}H^{\alpha}$, ^{15}N, $^{13}C^{\alpha}$, and $^{13}C'$ resonances were assigned using $^{1}H-^{15}N$ HSQC (Figure 1), HNCO, HN(CA)CO, HNCA, HN(CO)CA, CBCANH, CBCA(CO)NH, and $^{1}H-^{15}N$ HSQC-TOCSY experiments, and side chain ^{1}H and ^{13}C resonances were assigned using $^{1}H-^{15}N$ HSQC-TOCSY and HCCH-TOCSY experiments. Interproton distance restraints were derived from three-dimensional $^{1}H-^{13}C/^{15}N$ HSQC-NOESY experiments with mixing times of 75 and 150 ms; a particular $^{1}H-^{13}C$ HSQC-NOESY experiment was performed with the ^{13}C frequency carrier set to 150 ppm (corresponding to the aromatic carbons) and mixing times of 70 ms, for assignment of the aromatic protons. NOE

cross-peaks were classified as strong, medium, weak, and very weak, and converted into upper limits of 2.5, 3.5, 5.5, and 6.5 Å, respectively. Restraints involving pseudoatoms were systematically overestimated.

Backbone ϕ and ψ dihedral restraints were derived from TALOS (*12*) using as input the ^{1}H, ^{13}C, and ^{15}N backbone chemical shifts determined previously. Only TALOS prediction with 10 matches agreeing was used as ϕ and ψ dihedral restraints which are fixed by the average values with a standard deviation range with a minimum of 10°. All peptide bonds were kept planar and trans, with the exception of that between Met_{80} and Pro_{81} which was restrained to be planar and cis on the basis of the observation of a strong $C^{\alpha}H(i)-C^{\alpha}H(i+1)$ NOE between Met_{80} and Pro_{81} (*13*), and C^{β} and C^{γ} chemical shifts of Pro_{81} ($\delta_{C^{\beta}} = 34.86$ ppm, $\delta_{C^{\gamma}} = 25.56$ ppm) (*14*).

^{1}H−^{15}N HSQC experiments were performed at different temperatures (279.2, 284.7, 289.2, 294.9, 299.6, and 305.4 K) to determine the temperature coefficient ($\Delta\delta/\Delta T$) for each observable H^N on the ^{1}H−^{15}N HSQC spectra. This method permits us to include *a priori* experimental hydrogen bond restraints in the calculation on the basis of a weak observed temperature coefficient (*15*) correlating with the secondary structure prediction (see Table S1 of the Supporting Information for details about temperature coefficients). Hydrogen bond restraints were treated as two distance restraints with an upper limit of 2.4 Å between the hydrogen and the acceptor heavy atom and an upper limit of 3.5 Å between the acceptor and donor heavy atoms. Experimental restraints are summarized in Table 1.

Structure Calculations. Initial structures were calculated with DYANA (*16*). Three hundred randomized structures were generated, and simulated annealing calculations were performed with DYANA. The five structures with the lowest target function were selected for refinement.

The structures were refined by a minimization protocol using DISCOVER (Accelrys Inc., San Diego, CA) and the cvff force field (*17*) with a distance-dependent dielectric constant set to 4*r*, by means of 100 steps of steepest descent followed by 10 000 steps of a conjugate gradient algorithm. The five minimized structures were used as starting structures for restrained molecular dynamics at 300 K; after an equilibration period of 200 ps, each of the five structures was recorded every 5 ps over the course of 50 ps to generate 50 structures. The 20 best-fitting structures were selected as the final set. An arithmetic average was computed with MOLMOL (*18*) to describe the mean structure. Tables and figures were created using DYANA, MOLMOL, PROCHECK-NMR (*19*), and INSIGHT II. The coordinates of the 20 final structures have been deposited in the Brookhaven Protein Data Bank as entry 1TI3.

RESULTS

NOE Assignments and Structure Determination. After the required backbone and side chain ^{1}H, ^{13}C, and ^{15}N assignments had been made (*9*), the three-dimensional HSQC-NOESY spectrum was examined. A first set of approximately 900 unambiguous restraints (including dihedral restraints and hydrogen bonds stabilizing evident secondary structure elements) allows us to define the overall topology of PtTrx*h*1. Taking this topology into account, we then found it easier to assign ambiguous correlations and to identify the heavy atom acceptor for H^N exhibiting a low temperature coefficient (as $H^{N\xi 1}{}_{37}$ or $H^{N}{}_{41}$), and to gather the final set of 1906 distance restraints used for the calculation procedure described below (NOEs are represented in Figure 2).

Table 1: NMR-Derived Geometrical Restraints and Structural Statistics of the Conformational Ensemble

restraint	number
upper interproton	
total of distance restraints	1906
H-bonds[a]	122
intramolecular	894
sequential (i, $i+1$)	663
long-distance	217
dihedral angle	138
φ	67
ψ	70
ω[b]	1

violation	no. per conformer
distance violation (Å)	
>0.0	81 ± 9
>0.1	1.6 ± 1.4
>0.2	0
dihedral violation	
>0°	18 ± 3
>5°	2.1 ± 1.4
>10°	0
Ramachandran plot of residues[c]	
residues in the most favorable region (%)	79
residues in additional allowed regions (%)	19
residues in generously allowed regions (%)	2
residues in disallowed regions (%)	0

atoms	rmsd (Å)
backbone (residues 3−111)	0.53 ± 0.10
backbone (residues 1−113)	0.60 ± 0.12
heavy (residues 3−111)	0.89 ± 0.15
heavy (residues 1−113)	0.96 ± 0.18

[a] Each hydrogen bond is treated as two distance restraints, so 122 distance restraints represent 61 hydrogen bonds. [b] Only the cis peptide bond ($Met_{80}-Pro_{81}$), experimentally characterized, has been imposed. [c] Calculated with PROCHECK-NMR.

Structural Statistics. The 20 final structures of reduced PtTrx*h*1 exhibit an atomic rms distribution about the mean coordinate positions of 0.5 ± 0.1 Å for the backbone atoms and 0.90 ± 0.15 Å for all of the heavy atoms, excluding the two N- and C-terminal residues, which are ill-defined. The restrained molecular dynamics protocol has the advantage of offering a dynamic view of the structure, and most of the restraint violations are less than 0.1 Å. The structure set fits the experimental restraints with no interproton distance and torsion angle violations greater than 0.2 Å and 10°, respectively (Table 1). As shown in Figure 3, the rms distribution is not homogeneous along the sequence, which indicates a degree of flexibility in some regions (loops or turns). All of the backbone torsion angles of the non-glycine residues fall in the allowed regions of the Ramachandran plot, with the exception of Lys_{90} which is implicated in the β-bulge (Table 1).

Description of the Overall Structure. The overall structure of PtTrx*h*1 adopts a classical Trx fold that consists of a five-stranded β-sheet surrounded by four α-helices. Figure 4A shows the superposition of the 20 backbone structures and a schematic view of the regular secondary elements of the most representative structure. Approximately 80% of the

FIGURE 2: Summary of the sequential NOE connectivities in the reduced form of thioredoxin *h*1 from poplar. For the NN, αN, *β*N, and *αβ* nearest-neighbor connectivities, the NOE intensities are represented by different line thicknesses and are classified as strong, medium, weak, and very weak.

residues in PtTrx*h*1 are involved in regular secondary structures. The noncanonical active site forms a protruding loop from the end (Ala_{35}) of the second *β*-strand to the beginning (Lys_{42}) of helix α_2.

Hydrogen Bonding. Most of the imposed hydrogen bonds are present in the structure with a frequency greater than 80%. Four other important bonds are observed; the $H^N_{54}\cdots O_{51}$ bond, which appears in 70% of the calculated structures, is certainly due to the local disorder at the last turn of helix α_2 that generates a bifurcated hydrogen bond for H^N_{54}. The $H^{\gamma}_{82}\cdots O_{79}$ hydrogen bond (55% occurrence) seems to stabilize the loop between α_3 and β_4. The $H^N_{89}\cdots O_{87}$ bond, which participates to the loop between the β_4 and β_5 strands, and the $H^N_4\cdots O_{52}$ hydrogen bond are certainly modeling artifacts due to the absence of an explicit solvent; in fact, these two latter H^N protons present high temperature coefficients that are incompatible with the presence of hydrogen bonding (-9.3×10^{-3} and -7.13×10^{-3} ppm/K, respectively).

β-Sheet. The core of PtTrx*h*1 consists of a five-stranded *β*-sheet. The individual strands comprise residues from Val_6 to Cys_9 (β_1), Leu_{28} to Thr_{34} (β_2), Val_{58} to Asp_{64} (β_3), Thr_{82} to Lys_{87} (β_4), and Val_{92} to Val_{96} (β_5), this last strand being interrupted by the *β*-bulge (from Lys_{90} to Val_{92}). Both parallel (p) and antiparallel (a) arrangements of the strands display the pattern β_1(p)β_3(p)β_2(a)β_4(a)β_5. H^N_{65} forms a hydrogen bond with O_{34} that would allow us to include Val_{65} in β_3, but the dihedral angles ($\varphi = -54.4 \pm 5.5°$ and $\psi = -38.5 \pm 7.3°$) suggest that Val_{65} should belong to a type III *β*-turn from Val_{65} to Leu_{68} stabilized by the $H^N_{68}\cdots O_{65}$ hydrogen bond [this turn is characterized by the strong αN(65,68) NOE correlation]. The *β*-sheet has the characteristic right-handed twist.

Helices. PtTrx*h*1 contains four α-helices surrounding the *β*-sheet core. The first helix, α_1, extends from Val_{12} to Gly_{22} with three turns of regular α-helix. The second helix, α_2, is also regular and extends from Pro_{39} to Lys_{54} (including the $Pro_{39}-Cys_{41}$ fragment of the active site). A small distortion in the axis of this helix is caused by Pro_{46}, and this helix displays a regular helical hydrogen bond network with four turns. The third α-helix, α_3, extends from Lys_{69} to Asn_{76} with two turns of regular α-helix. The fourth and last α-helix, α_4, extends from Gly_{102} to His_{110}, with two regular turns and with the three final residues irregularly included as an incomplete turn because of the significant flexibility of that segment (shown by an important rmsd, 0.7 ± 0.3 Å, on the last three residues) but with retention of the $H^N_{111}\cdots O_{107}$ hydrogen bond in 100% of the structures.

Active Site. PtTrx*h*1 possesses a noncanonical active site with the Ala_{35}-Ser_{36}-Trp_{37}-Cys_{38}-Pro_{39}-Pro_{40}-Cys_{41}-Lys_{42} sequence, which is very well defined with a local backbone rmsd of 0.4 ± 0.1 Å (0.5 ± 0.1 Å for heavy atoms). As shown in Figure 4C, the active site forms a protruding loop outside the protein; residues $Ala_{35}-Cys_{38}$ are located on the

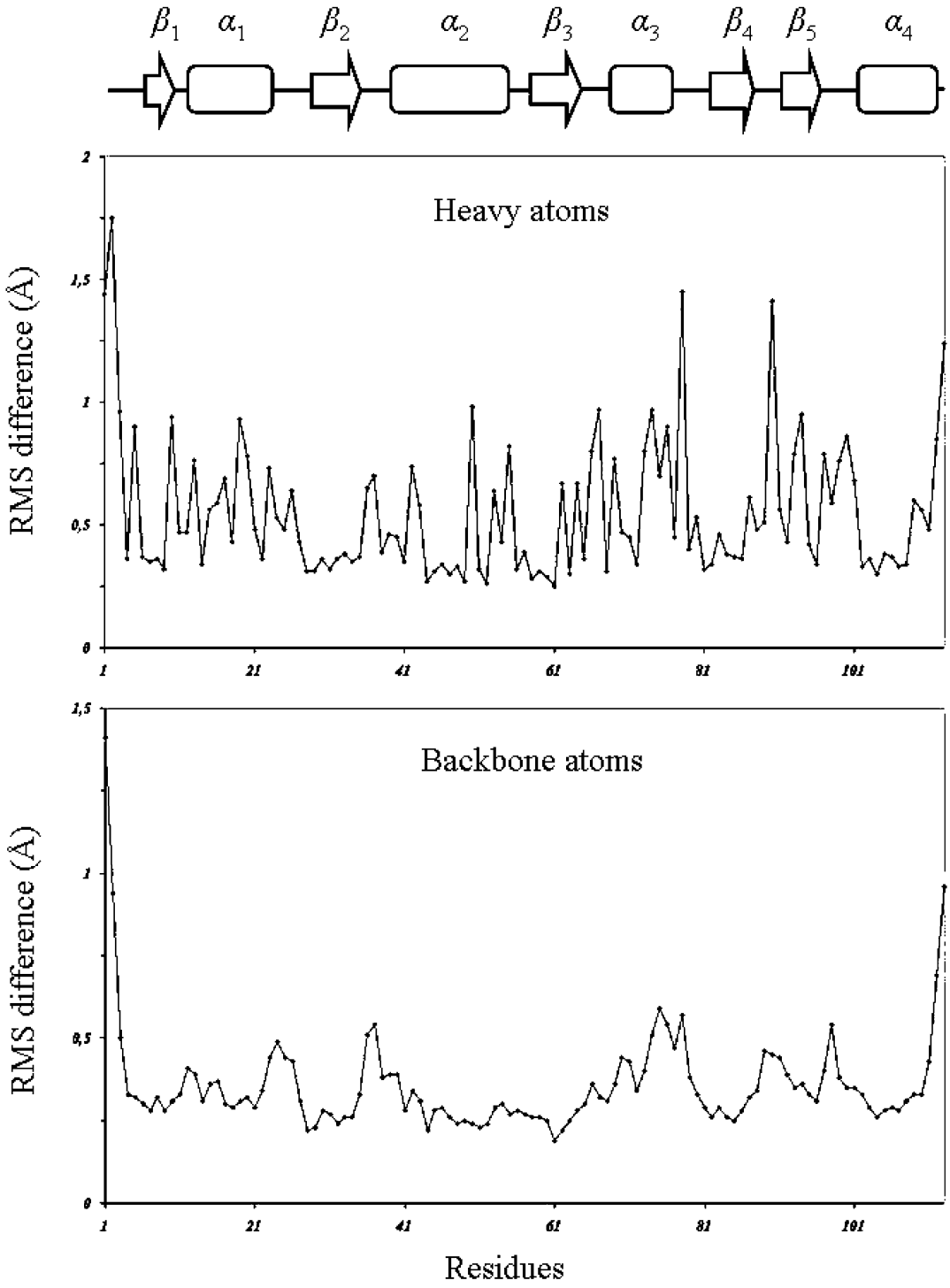

FIGURE 3: Root-mean-square distribution along the sequence. The rms distribution is not homogeneous along the sequence, reflecting flexibility of some regions, i.e., loops or turns between secondary structure elements.

loop between β_2 and α_2 and residues $Pro_{39}-Lys_{42}$ initiating the first turn of α_2 which is stabilized by both $H^N{}_{42}\cdots O_{38}$ and $H^N{}_{43}\cdots O_{39}$ hydrogen bonds. The aromatic ring of Trp_{37} is on the protein surface and interacts with its spatial neighboring residues (Ala_{35} and Met_{80}), a strong hydrogen bond between $H^{\xi}{}_{37}$ and $O^{\delta}{}_{66}$ ($H^{\xi}{}_{37}$ exhibits a temperature coefficient near 0 ppb/K) being observed in 90% of the structures. Cys_{38} and Cys_{41} are in their sulfhydryl form, and a hydrogen bond between $H^N{}_{41}$ and $S^{\gamma}{}_{38}$ is found in 100% of the structures ($H^N{}_{41}$ exhibits a small temperature coefficient of -1.8×10^{-3} ppm/K), stabilizing the spatial structure of the active site. Asp_{32}, which is supposed to facilitate the thiol deprotonation of Cys_{41} (*20*), is correctly located on strand β_2 (see Table S2 of the Supporting Information for the statistical data about the active site).

Aromatic Side Chains. Eight aromatic residues contribute to the structural stability of the protein hydrophobic core: Trp_{15} (which is specific to class I of thioredoxin *h*) (*4*), His_{18}, Phe_{33}, Phe_{48}, Phe_{60}, and Trp_{75} (which is specific to plant thioredoxin *h*, and not found in Trx*h* from *C. reinhardtii*, for example), Phe_{83}, and Phe_{85}. As shown in Figure 5A, residues Phe_{33}, Phe_{60}, Phe_{83}, and Phe_{85} are located on the inner side of the β-sheets and His_{18} and Phe_{48} are situated on the inner side of amphipathic helices and interact within

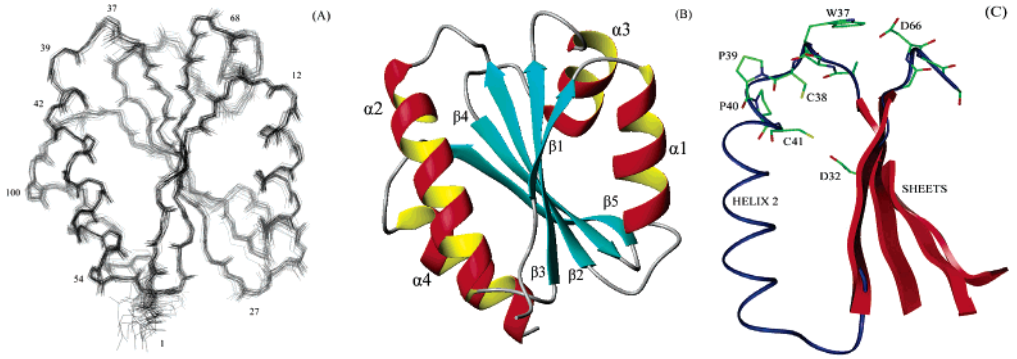

FIGURE 4: Overall solution structures of PtTrx*h*1 and its active site. (A) Backbone superposition of the ensemble of 20 structures. (B) Symbolic representation of the different secondary structure elements. (C) Active site of the most representative form (essential amino acids are represented with their side chains).

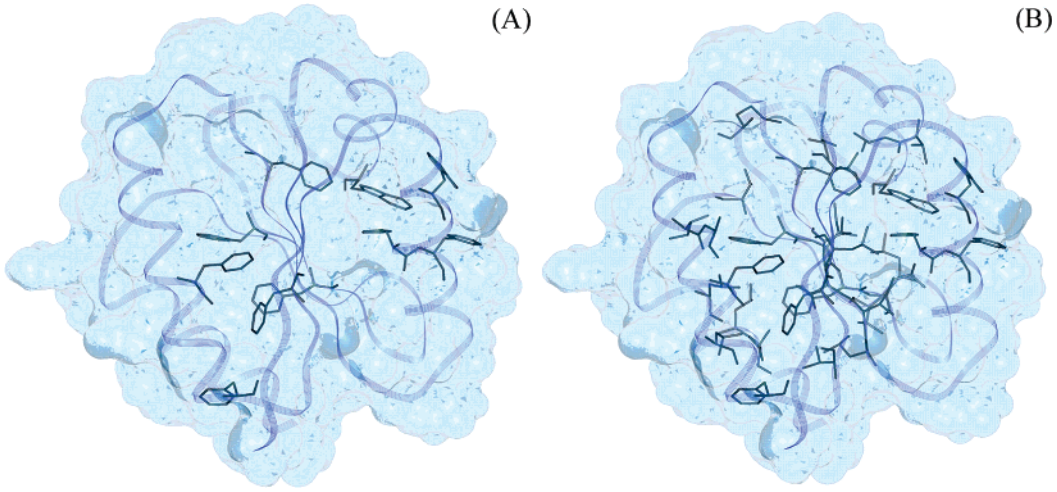

FIGURE 5: Hydrophobic core organization of PtTrx*h*1. (A) Aromatic side chains involved in the hydrophobic core are those of Trp_{15}, His_{18}, Phe_{19}, Phe_{33}, Phe_{48}, Phe_{55}, Phe_{60}, Trp_{75}, Phe_{83}, and Phe_{85}. (B) Aromatic and aliphatic side chains involved in the hydrophobic core are those of Leu_{28}, Ile_{29}, Val_{30}, Val_{31}, Ile_{44}, Leu_{51}, Val_{58}, Leu_{61}, Val_{63}, Leu_{68}, Ile_{84}, Leu_{86}, Leu_{91}, Val_{92}, Val_{96}, Leu_{103}, Leu_{106}, and Val_{107}.

the hydrophobic core. Trp_{15} and Trp_{75} interact with one another (and certainly with His_{18}) in a groove formed by helices α_1 and α_3. Moreover, several NOE correlations can be observed between the two Trp_{15} and Trp_{75} side chains. In addition, Phe_{55}, which is conserved in thioredoxins (*21*), is positioned at the end of a groove formed by helices α_2 and α_4 and Phe_{19} in the groove between helices α_1 and α_3, near Trp_{15} and Trp_{75}. As shown in Figure 5B, other nonaromatic hydrophobic side chains participate in the hydrophobic core.

DISCUSSION

Comparison with Other Known Thioredoxin Structures. Thioredoxins can be quite divergent in their primary structures, although all of the structures resolved up to date adopt the Trx fold. In that context, it is interesting to compare our solution three-dimensional structure of PtTrx*h*1 with other well-known thioredoxins, the closest one being thioredoxin *h* from *C. reinhardtii* (CrTrx*h*1) (*8*).

The sequences of these two proteins are only 50% identical, although the overall tertiary structures are very close; the different secondary structure elements have the same size and position. As in human thioredoxin (*22*), the α_1 and α_3 helices are longer than in the bacterial thioredoxin and α_3 helix is clearly identified as a regular α-helix.

Also, some differences can be observed with the structure of thioredoxin *h* from *C. reinhardtii* (CrTrx*h*1), the N-terminus of PtTrx*h*1 being much longer than that of CrTrx*h*1 and freely exposed to solvent. The Lys_{23}−Lys_{27} loop of PtTrx*h*1 (located between α_1 and β_2) is quite different from the Lys_{21}−Lys_{25} loop of CrTrx*h*1. In the case of PtTrx*h*1, Lys_{23}−Lys_{27} form an irregular α-turn (stabilized by the $H^N{}_{25}\cdots O_{21}$ hydrogen bond) ending the α_1 helix; this loop interacts closely with the Asp_{88}−Leu_{91} one (extending from β_4 to β_5); for CrTrx*h*1, the Lys_{21}−Lys_{25} loop remains unstructured. The β-bulge is also more structurally defined in PtTrx*h*1 than in CrTrx*h*1, introducing slight conformational differences between the Asp_{88}−Leu_{91} (PtTrx*h*1) and Ap_{87}−Lys_{90} (CrTrx*h*1) loops.

It was reported that CrTrx*h*1 is less thermostable than PtTrx*h*1 (*5*). A closer examination of the structural differences between the two proteins might explain this observation. The first idea is that Trp_{75} contributes to the reinforcement of the hydrophobic core, thus increasing the thermal stability. Indeed, this residue is not present in CrTrx*h*1 (substituted for Ala), but an experimental A74Y mutation in CrTrx*h*1 did not change the thermal properties of this enzyme (*23*). The number of hydrogen bonds in each structure shows that the β-sheets in PtTrx*h*1 are stabilized by a greater number of hydrogen bonds than in CrTrx*h*1 (*24*), 25 instead of 20. This observation could explain the difference in thermal stability between these two proteins. Moreover, this observation supports the idea that this family

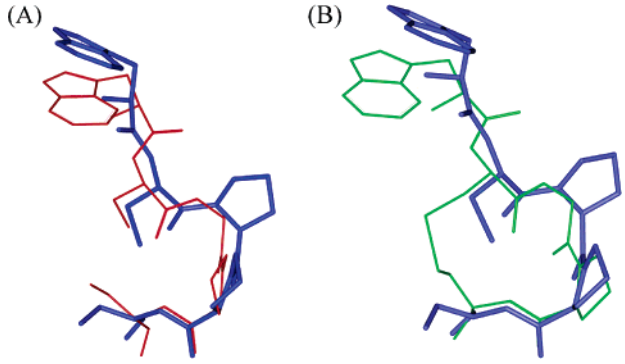

FIGURE 6: Active site comparisons. (A) Backbone superposition between the active site of PtTrx*h*1 (blue) and that of *E. coli* Trx (red) leads to a rmsd of 0.98 Å. (B) Backbone superposition with the active site of the oxidized CrTrx*h*1 (green) gives a rmsd of 1.14 Å.

of protein is more stabilized by the inner β-sheet disposition (and its hydrogen bonding network) than by hydrophobic packing forces.

As reported above, the PtTrx*h*1 active site is well-defined and consists of a protruding loop between β_2 and α_2, including the first turn of α_2. Backbone superposition between the active site of PtTrx*h*1 ($W_{37}C_{38}P_{39}P_{40}C_{41}$) and that of *E. coli* Trx ($W_{31}C_{32}G_{33}P_{34}C_{35}$) (*25*) leads to a rmsd of 0.98 Å as shown in Figure 6A. The same superposition with the active site of the oxidized CrTrx*h*1 give a rmsd of 1.14 Å as shown in Figure 6B. It has been reported that the difference between oxidized and reduced forms of a Trx from a given organism is negligible (*26*, *27*). Assuming that backbone position and side chain orientations of the PtTrx*h*1 active site are very close to that observed in classical thioredoxins, we can conclude that the G to P mutation does not give rise to important conformational changes but leads to more rigid structural characteristics. First, the presence of a second proline in the active site seems to decrease the flexibility of the loop as revealed by a low rmsd on the $Ala_{35}-Lys_{42}$ segment; second, the portion of the active site, included in the α_2 helix, adopts a more regular α-helical turn than in other structures where this turn is commonly considered to be rather loosely defined.

Structure−Function Relationship. As reported below, the atypical active site adopts a classical spatial disposition, suggesting that the conformation of the Cys-X-X-Cys loop is necessary for the redox activity. The presence of a proline instead of a glycine residue may play a singular role in specificity and/or in redox potential. No explanation can be formulated about structural determinants for PtTrx*h*1 specificity, but the characteristics induced by Pro and/or the chemical nature of the side chains surrounding the active site probably play an important role in specificity.

PtTrx*h*1 exhibits an important propensity to polymerize at high concentrations; this type of covalent aggregation may occur for the oxidized form of thioredoxin *h*, suggesting the formation of an intermolecular disulfide bridge involving a cysteine residue other than Cys_{38} or Cys_{41}. The only single cysteine (Cys_9) present in the PtTrx*h*1 sequence may participate to the formation of an intermolecular covalent bond. In fact, this cysteine is situated on strand β_1 and is relatively exposed to the solvent, a position in favor of the formation of a heterodisulfide bridge.

Thioredoxins *h* from subgroup I are found in the phloem sieve tubes. Since these proteins are synthesized in the companion cell, they are able to be transferred through plasmodesmata to the enucleate sieve tube elements (*28*). The N-terminal motif AEE, necessary for this cell to cell transfer, is a recognition sequence, and in agreement, it is largely exposed to solvent. It does not exhibit any particular conformation and seems to be particularly flexible except that the two glutamate side chains must face the solvent, allowing a possible protein−protein interaction. Moreover, the fourth following glycine residue in the sequence may increase the flexibility of the AEE fragment and its conformational adaptability.

CONCLUDING REMARKS

The solution structure of thioredoxin *h*1 from poplar described in this paper is the first reported structure of a higher-plant thioredoxin *h*. On the basis of the particularities of that protein, we have focused on the understanding of the structural determinants of its specificity and thermostability. Along with the similarities found between this protein and other thioredoxins, we showed its specific conformation to be mandatory for its redox activity. In that context, it will be of a great interest, by means of NMR studies, to investigate interaction mechanisms of different protein−protein complexes involving thioredoxin *h*1 with other in vivo partners such as NADP thioredoxin reductase (NTR) or glutaredoxin (GRX) (*29*).

ACKNOWLEDGMENT

Access to the Bruker DRX 600 NMR facilities of the Service Commun de Biophysicochimie des Interactions, Nancy I, is deeply appreciated. We thank Dr. G. Boussard for his critical review of the manuscript.

SUPPORTING INFORMATION AVAILABLE

Tables giving the temperature coefficients ($\Delta\delta/\Delta T$) of H^N involved in hydrogen bond restraints and the structural statistics about the $Ala_{35}-Lys_{42}$ active site. This material is available free of charge via the Internet at http://pubs.acs.org.

REFERENCES

1. Holmgren, A. (2000) Antioxidant function of thioredoxin and glutaredoxin systems, *Antioxid. Redox Signaling 2*, 811−820.
2. Elkund, H., Cambillau, C., Sjoberg, B. M., Holmgren, A., Jornvall, H., Hoog, J. O., and Branden, C. I. (1984) Conformational and functional similarities between glutaredoxin and thioredoxins, *EMBO J. 3*, 1443−1449.
3. Meyer, Y., Vignols, F., and Reichheld, J. P. (2002) Classification of plant thioredoxins by sequence similarity and intron position, *Methods Enzymol. 347*, 394−402.
4. Gelhaye, E., Rouhier, N. and Jacquot, J. P. (2004) The thioredoxin h system of higher plants, *Plant Physiol. Biochem. 42*, 265−271.
5. Behm, M., and Jacquot, J. P. (2000) Isolation and characterization of thioredoxin h from poplar xylem, *Plant Physiol. Biochem. 38*, 363−369.
6. Rivera-Madrid, R., Mestres, D., Marinho, P., Jacquot, J. P., Decottignies, P., Miginiac-Maslow, M., and Meyer, Y. (1995) Evidence for five divergent thioredoxin *h* sequences in *Arabidopsis thaliana*, *Proc. Natl. Acad. Sci. U.S.A. 92*, 5620−5624.
7. Brehelin, C., Mouaheb, N., Verdoucq, L., Lancelin, J. M., and Meyer, J. M. (2000) Characterization of determinants for the specificity of *Arabidopsis* thioredoxins *h* in yeast complementation, *J. Biol. Chem. 275*, 31641−31647.

8. Mittard, V., Blackledge, M. J., Stein, M., Jacquot, J. P., Marion, D., and Lancelin, J. M. (1997) NMR solution structure of an oxidised thioredoxin h from the eukaryotic green alga *Chlamydomonas reinhardtii*, *Eur. J. Biochem. 243*, 374−383.
9. Coudevylle, N., Thureau, A., Hemmerlin, C., Gelhaye, E., Jacquot, J. P., and Cung, M. T. (2004) ^{1}H, ^{13}C and ^{15}N resonance assignment of the reduced form of thioredoxin h1 from poplar, a CPPC active site variant, *J. Biomol. NMR 30*, 229−230.
10. Bartels, C., Xia, T., Billeter, M., Güntert, P., and Wüthrich, K. (1995) The program XEASY for computer-supported NMR spectral analysis of biological macromolecules, *J. Biomol. NMR 6*, 1−10.
11. Wishart, D. S., Bigam, C. G., Yao, J., Abildgaard, F., Dyson, H. J., Oldfield, E., Markley, J. L., and Sykes, B. D. (1995) ^{1}H, ^{13}C and ^{15}N chemical shift referencing in biomolecular NMR, *J. Biomol. NMR 5*, 135−140.
12. Cornilescu, G., Delaglio, F., and Bax, A. (1999) Protein backbone angle restraints from searching a database for chemical shift and sequence homology, *J. Biomol. NMR 13*, 289−302.
13. Forman-Kay, J. D., Clore, G. M., Driscoll, P. C., Wingfield, P., Richards, F. M., and Gronenborn, A. M. (1989) A proton nuclear magnetic resonance assignment and secondary structure determination of recombinant human thioredoxin, *Biochemistry 28*, 7088−7097.
14. Siemion, I. Z., Wieland, T., and Pook, K. H. (1975) Influence of the distance of the proline carbonyl from the beta and gamma carbon on the ^{13}C chemical shifts, *Angew. Chem., Int. Ed. Engl. 14*, 702−703.
15. Baxter, J. N., and Williamson, M. P. (1997) Temperature dependence of ^{1}H chemical shifts in proteins, *J. Biomol. NMR 9*, 359−369.
16. Guntert, P., Mumenthaler, C., and Wüthrich, K. (1997) Torsion angle dynamics for NMR structure calculation with the new program DYANA, *J. Mol. Biol. 273*, 283−298.
17. Dauber-Osguthorpe, P., Roberts, V. A., Osguthorpe, D. J., Wolff, J., Genest, M., and Hagler, A. T. (1988) Structure and Energetics of Ligand Binding to Proteins: *E. coli*. Dihydrofolate Reductase-Trimethoprim, A Drug-Receptor System, *Proteins: Struct., Funct., Genet. 4*, 31−47.
18. Koradi, R., Billeter, M., and Wüthrich, K. (1996) MOLMOL: A program for display and analysis of macromolecular structures, *J. Mol. Graphics 14*, 52−55.
19. Laskowski, R. A., Rullmann, J. A. C., MacArthur, M. W., Kaptein, R., and Thornton, J. M. (1996) AQUA and PROCHECK-NMR: Programs for checking the quality of protein structures solved by NMR, *J. Biomol. NMR 8*, 477−486.
20. Chivers, P. T., and Raines, R. T. (1997) General Acid/Base Catalysis in the Active Site of *Escherichia coli* Thioredoxin, *Biochemistry 36*, 15810−15816.
21. Eklund, H., Gleason, F. K., and Holmgren, A. (1991) Structural and functional relations among thioredoxins of different species, *Proteins: Struct., Funct., Genet. 11*, 13−28.
22. Forman-Kay, J. D., Clore, G. M., Wingfield, T. P., and Gronenborn, M. A. (1991) High-resolution three-dimensional structure of reduced recombinant human thioredoxin in solution, *Biochemistry 30*, 2685−2698.
23. Lemaire, S. D., Richardson, J. M., Goyer, A., Keryer, E., Lancelin, J. M., Makhatadze, G. I., and Jacquot, J. P. (2000) Primary structure determinants of the pH- and temperature-dependent aggregation of thioredoxin, *Biochim. Biophys. Acta 1476*, 311−323.
24. Mittard, V., Morelle, N., Brutscher, B., Simorre, J. P., Marion, D., Stein, M., Jacquot J. P., Lirsac P. N., and Lancelin, J. M. (1995) ^{1}H, ^{13}C, ^{15}N resonance assignments oxidized thioredoxin *h* from the eukaryotic green alga *Chlamydomonas reinhardtii* using new methods based on 2D triple-resonance NMR spectroscopy and computer assisted backbone assignment, *Eur. J. Biochem. 229*, 473−485.
25. Dyson, H. J., Gippert, G. P., Case, D. A., Holmgren, A., and Wright, P. (1990) Three-dimensional solution structure of the reduced form of *Escherichia coli* thioredoxin determined by nuclear magnetic resonance spectroscopy, *Biochemistry 29*, 4129−4136.
26. Jeng, M. F., Campbell, A. P., Begley, T., Holmgren, A., Case, D. A., Wright, P. E., and Dyson, H. J. (1994) High-resolution solution structures of oxidized and reduced *Escherichia coli* thioredoxin, *Structure 2*, 853−868.
27. Couprie, J., Remerowski, M. L., Bailleul, A., Courcon, M., Gilles, N., Quemeneur, E., and Jamin, N. (1998) Differences between the electronic environments of reduced and oxidized *Escherichia coli* DsbA inferred from heteronuclear magnetic resonance spectroscopy, *Protein Sci. 7*, 2065−2080.
28. Ishiwatari, Y., Honda, C., Kawashima, I., Nakamura, S., Hirano, H., Mori, S., Fujiwara, T., and Chino, M. (1995) Thioredoxin *h* is one of the major proteins in rice phloem sap, *Planta 195*, 456−463.
29. Tamarit, J., Belli, G., Cabiscol, E., Herrero, E., and Ros, J. (2003) Biochemical Characterization of Yeast Mitochondrial Grx5 Monothiol Glutaredoxin, *J. Biol. Chem. 278*, 25745−25751.

BI047816N